Analytica Chimica Acta 1150 (2021) 338232

Contents lists available at ScienceDirect

Analytica Chimica Acta

journal homepage: www.elsevier.com/locate/aca

Label-free chemiresistor biosensor based on reduced graphene oxide and *M13* bacteriophage for detection of coliforms

Kenta Nakama [a, b, 1], Mohammed Sedki [c, 1], Ashok Mulchandani [a, d, *]

[a] Department of Chemical and Environmental Engineering, University of California, Riverside, CA, 92521, USA
[b] Department of Biotechnology and Life Science, Tokyo University of Agriculture and Technology, 2-24-16 Naka-cho, Koganei, Tokyo, 184-8588, Japan
[c] Materials Science and Engineering Program, University of California, Riverside, CA, 92521, USA
[d] Center for Environmental Research and Technology (CE-CERT), University of California, Riverside, CA, 92507, USA

GRAPHICAL ABSTRACT

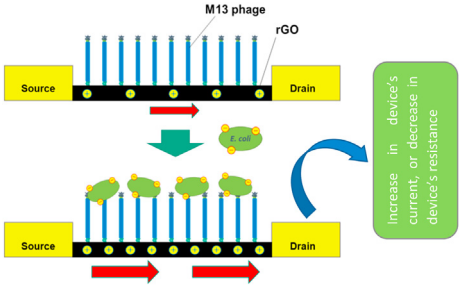

ARTICLE INFO

Article history:
Received 9 October 2020
Received in revised form
12 January 2021
Accepted 14 January 2021
Available online 21 January 2021

Keywords:
Phage biosensor
Filed-effect transistor
Graphene
Detection of bacteria
M13-rGO-FET
Electrical sensor

ABSTRACT

Coliform bacteria are well known as informative indicators for bacterial contamination in water. This study presents a novel chemiresistor biosensor using *M13* phage-modified reduced graphene oxide (rGO) for detection of *Escherichia coli* (*E. coli*), as coliform bacteria. *M13* phage, as a biorecognition element, was immobilized on the rGO channel, so that it can bind to negatively charged *E. coli* bacteria, allowing the gating effect on the biosensor and the change in its resistance. The prepared materials and device were characterized using spectroscopic, microscopic, and electrical measurements. FTIR and XRD results proved the successful fabrication of GO and rGO nanosheets. AFM results showed that the prepared nanosheets were monolayer. The SEM micrographs of the *M13*-functionalized devices, soaked in two different concentrations of *E. coli*, confirmed the successful capturing of *E. coli* and that the signal change is concentration-dependent. As a result, a linear and specific response towards *E. coli* was observed and the limit of detection was determined to be 45 CFU/mL. Further, the proposed sensor system showed selectivity towards the tested coliforms. These results suggested this sensing system could be a promising tool for detecting coliforms with an economic, accurate, rapid, and directly applicable process.

* Corresponding author. Department of Chemical and Environmental Engineering, University of California, Riverside, CA, 92521, USA.
E-mail address: adani@engr.ucr.edu (A. Mulchandani).
[1] Equal contribution.

https://doi.org/10.1016/j.aca.2021.338232
0003-2670/

1. Introduction

Fecal coliforms have received a widespread attention as typical biomarkers for water contamination with bacteria [1]. There are several methods used for detection of coliform. The first is a basic colony counting method [2]. While simple, the method takes a long time for getting results, usually more than 24 h. Other methods used in laboratory are based on the principle of ELISA or PCR [3,4]. These methods require specific reagents and instruments for the detection, making the processes expensive and time-consuming, besides the need for trained professionals [5,6]. Biosensors have been developed as economic and more promising tools for identifying coliforms. They offer simple operation and rapid response with accuracy, but still need further optimization and standardization for application. Phages are of a great importance as bioreceptors in biosensors [7,8].

Here, M13 bacteriophage was implemented as a biorecognition element for coliform detection. M13 phage is a non-lytic bacterial virus which infects and grows only in the male strains of *Escherichia coli* (*E. coli*) by recognizing its F-pili [9]. In addition, M13 phage is more stable against the change of pH or temperature, compared to other biorecognition elements such as antibodies [10]. In addition, it is economic and easy to prepare by simple bacterial cultivation methods.

Amongst the different transducers, biosensors based on chemiresistor (CR) are receiving a great deal of attention in recent years for label-free biosensing with a facile procedure [11–15]. CR biosensor is a sensor in which the resistance of the device changes as a result of the changes of its nearby chemical environment. Generally, when biomolecules with electrical charges are near the semiconductor channel, they provide the electrostatic gating effects to the sensing platform, changing the number of charge carriers in the semiconductor channel and thereby the resistance of the CR sensor [16].

Reduced graphene oxide (rGO) is a well-known nanomaterial utilized in a wide range of applications, including sensors. It has a large surface area, which is available for direct interaction with a variety of biomolecules and whole cells [17–19]. Our research group has conducted a detailed study (publication in progress) of the parameters that affect the quality of GO/rGO, which had led to obtaining pristine graphene-like rGO, which improved its charge transport and electronic properties.

This study aims to develop a label-free CR biosensor using M13 bacteriophage and rGO for detecting fecal coliform. We focused on *E. coli* bacteria as biomarker for indicating the presence of bacterial contamination in river water and M13 phage as a biorecognition molecule. This sensor exhibited good sensitivity and low limit of detection (LOD) of 45 CFU/mL, which is comparable with previous reports. Furthermore, the specificity and applicability of this biosensor are also demonstrated using *Pseudomonas chlororaphis* (*P. chlororaphis*) strain, as non-host bacteria, and simulated river water sample, respectively.

2. Materials and methods

2.1. Materials

Graphite flakes, phosphoric acid (H_3PO_4, 85%), sulfuric acid (H_2SO_4, 98%), potassium permanganates ($KMnO_4$, 99%), hydrochloric acid (HCl, 37%) and hydrogen peroxide (H_2O_2, 30%) were all purchased from Fisher Scientific, USA. (3-Aminopropyl) triethoxysilane (APTES) was bought from Sigma (St. Louis, MO, USA). 1-pyrene carboxylic acid (PCA), dimethylformamide (DMF), Tween 20 (T20), 1-ethyl-3-(3-dimethylaminopropyl) carbodiimide hydrochloride (EDC), and N-hydroxysuccinimide (NHS) were all purchased from Sigma Aldrich (St. Louis, USA). Ethanolamine (EA) was acquired from Acros Organic-Fisher Scientific.

2.2. Materials synthesis and characterization

The bacteria solution of *E. coli XL1-blue* and *Pseudomonas chlororaphis* were cultured in LB media by the same way as our previous report. In addition, M13 bacteriophage was prepared same as our previous work [10].

GO nanosheets were prepared as illustrated in our previously published work [20]. The prepared GO and rGO nanosheets were characterized using X-ray diffraction (XRD, PANalytical Empyrean Series 2), Fourier transform infra-red (FTIR, Thermo Nicolet 6700)

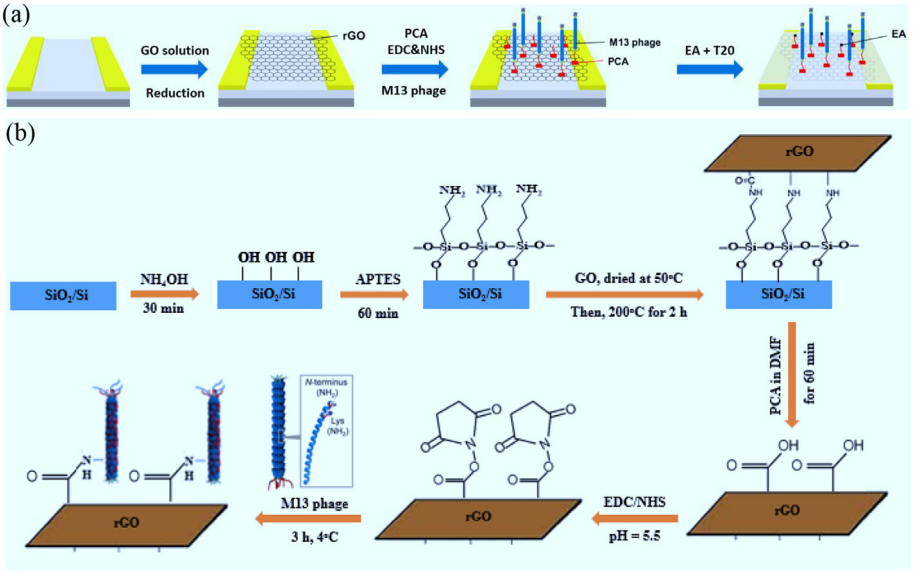

Fig. 1. Sensors fabrication. (a) Schematic diagram of the preparation procedures of rGO-M13 phage-based biosensor. (b) A more detailed schematic showing the chemistry of sensor fabrication. The red dots on M13 phage represent the amine groups positions. (For interpretation of the references to colour in this figure legend, the reader is referred to the Web version of this article.)

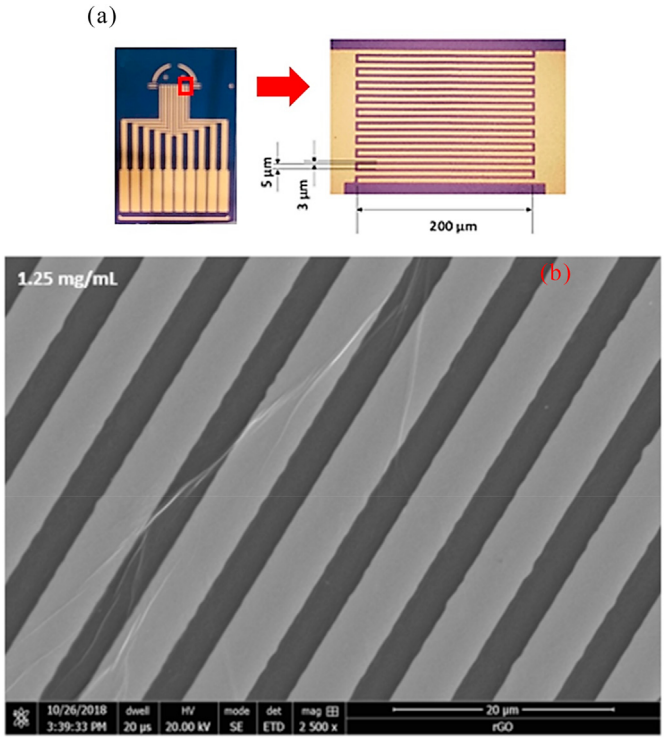

Fig. 2. The sensor system design. (a) Phone camera image of the gold interdigitated electrodes (device). (b) SEM image of the device with a thin film of rGO. (For interpretation of the references to colour in this figure legend, the reader is referred to the Web version of this article.)

spectroscopy, atomic force microscopy (AFM, Horiba LabRam/AIST-NT), and scanning electron microscopy (SEM, ThermoFisher Scientific (formerly FEI/Philips) NNS450).

All electrical measurements were performed using the Keithley 2636 System Source Meter® (Tektronix, Beaverton, OR, USA).

2.3. Fabrication of the biosensor

Fig. 1 illustrates a schematic of the fabrication protocol of M13-rGO biosensor. The interdigitated gold electrodes (chips), shown in Fig. 2a, were fabricated on a p-type silicon substrate with a 300 nm SiO_2 insulating oxide layer deposited on top. Electrodes were patterned on the Si/SiO_2 substrate by conventional photolithography. Then, Cr (5 nm) and Au (50 nm) layers were deposited on the substrate using e-beam evaporation. Each device has 5 pairs of source and drain interdigitated gold electrodes with 5 µm width separated by 3 µm gaps of SiO_2 insulating layer. We used rGO to bridge the gaps of interdigitated gold electrodes.

The interdigitated gold electrodes written on Si/SiO_2 wafers were cleaned sequentially with acetone, isopropanol, methanol and deionized water (DI water) followed by drying with air. The electrodes were first incubated with 30% ammonium hydroxide for 30 min to introduce hydroxyl groups, and then incubated with APTES for 60 min. 15 µL of 1.25 mg/mL GO solution were dropped onto the interdigitated electrodes and dried at 50 °C for 30 min. Subsequently, the interdigitated electrodes with GO were annealed at 200 °C for 120 min in ambient air. The electrodes were further incubated with 100 mM PCA dissolved in DMF for 60 min, washed with DMF, and dried with N_2 gas. After that, the electrodes were incubated with 6.0 mM EDC and 6.0 mM NHS in 100 mM 2-(N-morpholino) ethanesulfonic acid (MES) buffer (pH 5.5), each for 20 min to activate the carboxylic groups, followed by incubation with 25 µL of M13 phage solution at 4 °C for 3 h. Then the electrodes were incubated with 100 mM EA for 30 min to passivate residual ester groups of NHS and rinsed thoroughly with 10 mM sodium phosphate buffer (PB, pH 7.4), followed by incubation with 1.0% (v/v) T20 for 30 min to block the bare rGO on the electrodes. The chips were washed with the proper buffer after each of the previous modification steps.

The fabrication steps were monitored by measuring the device's resistance after each step. The device's resistance was determined from the slopes of current-voltage (I–V) curves between V_{SD} of +0.1 V and −0.1 V.

2.4. Sample measurement using prepared biosensor

Sensing procedure consisted of measuring the initial resistance (R_0) of the sensor (determined from the slopes of I–V curves between +0.1 V and −0.1 V) followed by incubation for 30 min with 25 µL of different concentrations of *E. coli XL1-blue* solution, rinsing 3 times with PB and measuring the resistance (R) again. Percentage changes $(R-R_0)/R_0$% were plotted as a function of log value of *E. coli* concentration to evaluate the sensor performance characteristics. The same sensors were used for the whole range from 10^2 to 10^7 CFU/mL.

3. Results and discussions

3.1. Materials characterization

Fig. 2b shows the SEM image of the interdigitated gold electrodes with rGO. As shown in the figure, the very thin rGO film totally covered the interdigitated gold electrodes gaps in the sensing area. The strong immobilization of rGO thin film on the substrate is attributed to the chemical bonds' formation between APTES and rGO, Fig. 1b, which was explained in detail by Ou et al. [21], where epoxy groups from GO encounter ring opening and bind to primary amine groups (-NH_2), which convert into secondary amines (−NH−). On the other hand, amide bond formation between carboxyl groups (-COOH) and −NH_2 are less likely to happen in the absence of coupling agents such as EDC/NHS, at room temperature. However, in this case zwitterionic COO−NH3$^+$

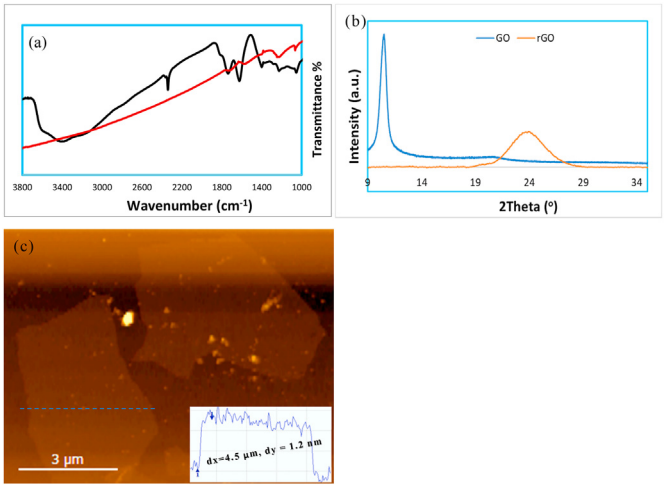

Fig. 3. The spectroscopic characterizations of GO and rGO nanosheets. (a) FTIR spectra of GO (black) and rGO (red) nanosheets. (b) XRD analysis showing sharp peak of GO at 2 theta = 10.4°, and rGO with a diffraction peak centering at 24°. (c) AFM image of GO with its height profile. (For interpretation of the references to colour in this figure legend, the reader is referred to the Web version of this article.)

linkages are formed, that under the effect of heat (200 °C) form −CO−NH- (amide) linkages.

The prepared GO, and rGO nanosheets were characterized by FTIR spectroscopy as shown in Fig. 3a. In GO sample, the stretching vibrational peaks of hydroxyl groups, carbonyl groups, and C=C double bonds appeared at 3400 cm^{-1}, 1722 cm^{-1}, and 1627 cm^{-1}, respectively [22]. The thermal reduction of GO nanosheets at 200 °C and ambient conditions could remove most of the hydroxyl and the carbonyl groups, and that is clear from the significant decrease in their peak strengths. These results comply with literature [23]. The thermal reduction process can be understood as a degassing process, where most of the oxygen functionalities get removed in the form of CO_2 and water vapor, which in turn helps remove the foreign atoms (oxygen) and convert more sp^3 carbons into sp^2 ones [20,24,25]. Hence, the electrical properties of GO get strongly improved by thermal reduction into rGO.

The XRD patterns, Fig. 3b., were recorded using Cu Kα radiation ($\lambda = 1.54$ °A) at 45 kV and 40 mA, and in the range of $2\Theta = 9^o$–44°. From Bragg's law ($n\lambda = 2d \sin(\Theta)$), graphite has a d-spacing between its graphene sheets of around 0.34 nm ($2\Theta = 26^\circ$), corresponding to the (002) planes. Due to the oxide functionalities, GO sheets were pushed further from each other, with a longer d-spacing (d ≈ 0.84 nm), corresponding to a smaller diffraction angle of $2\Theta = 10.5^\circ$. By thermal reduction of GO into rGO, the (002) peak shifts to a slightly broader peak at $2\Theta = 24^\circ$, corresponding to a smaller d-spacing of ≈0.37 nm. The decrease of d-spacing is attributed to the removal of oxygen functionalities in the reduction process [26].

The thickness, which determines the number of layers, of the prepared GO nanosheets was determined using AFM imaging. The height profile in Fig. 3c shows that the thickness is 1.2 nm, which corresponds to single layer GO. This thickness is larger than that of single-layer graphene (0.4 nm), as it includes the extra height coming from oxygen functionalities in GO, which pushes the sheet further from the substrate [26–30].

3.2. Monitoring of device modifications using I–V measurements

After each modification step, the resistance of the sensor was measured (determined from the slopes of I–V curves between +0.1 V and −0.1 V) for monitoring the modification steps. As shown in Fig. 4, there were linear I–V curves, indicating Ohmic contact between the Au-electrodes and the overlaying rGO thin film. The resistance of the sensor chip increased after each modification step of PCA, EDC/NHS-M13 phage, EA, and T20, compared to the interdigitated electrodes with rGO. Especially, the change in resistance of the sensor chip was large after the modification steps of PCA and EDC/NHS-M13 phage. These results suggest that the large molecules modified on the electrodes increased their resistance. On the other hand, small changes in resistance were observed after the modification steps of EA and T20. These results are consistent with literature, confirming that the modification steps of the sensor chip were successful [16].

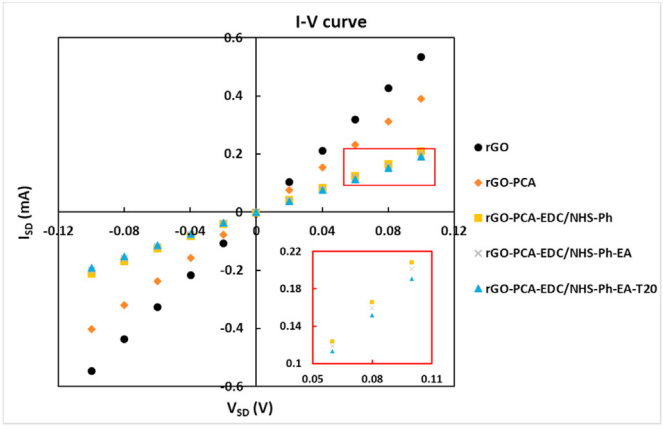

Fig. 4. The fabrication steps were confirmed by monitoring I–V curves between source and drain, at a V_{SD} of +0.1 V and −0.1 V. The resistance of the sensor system increased after each modification step of PCA, EDC/NHS-M13 phage, EA, and T20, compared to the interdigitated electrodes only with rGO.

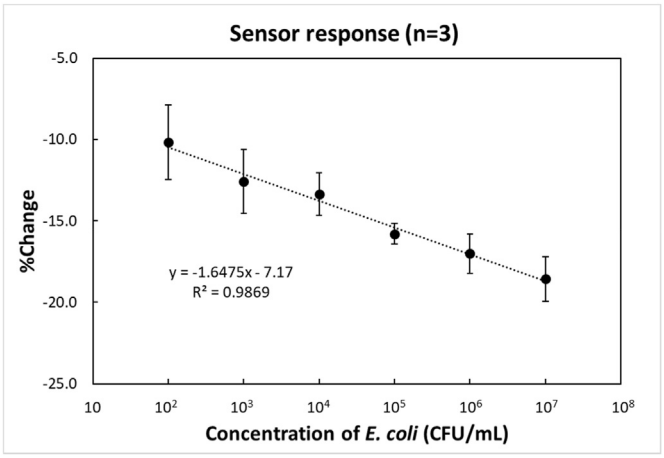

Fig. 5. Calibration curve plotting % resistance change ($(R-R_0)/R_0$%) against the concentration of *E. coli*. R_0 is the resistance of the M13-modified rGO channels after incubation with PB and R is the resistance of the sensor after incubation with different concentrations of *E. coli*. Each data point is an average of responses from 3 different M13-modified sensors and error bars represent ±1 standard deviation.

3.3. Measurement of E. coli bacteria

The biosensors were evaluated for *E. coli* detection by incubation with 10^2 CFU/mL to 10^7 CFU/mL. The sensor response (% resistance change calculated as $(R-R_0)/R_0*100 = \Delta R/R_0*100$, where R_0 is the sensor's resistance before the addition of *E. coli* bacteria, and R is

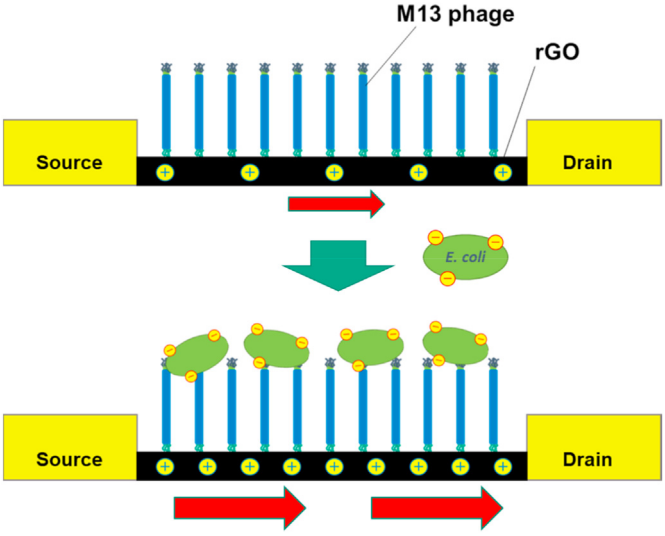

Fig. 6. The sensing mechanism of the rGO-M13 phage CR-FET biosensor for *E. coli* detection. Illustration of the change of the charge distribution induced by the binding of the negatively charged *E. coli*.

Table 1
Comparison of the sensing performance for various detection methods.

Method	Detection time	Bacteria	Detection limit	Reference
Flow cytometry	5 min	*E. coli* and others	10^5 cells/mL	[31]
PCR	4 h	*Listeria* and others	10^3 CFU/mL	[32]
Fluorescence	20 min	*E. coli*	50.2 CFU/mL	[33]
Antibody-G-FET	100 s	*E. coli*	10 CFU/mL	[34]
Aptamer-G-FET	72 s	*E. coli*	10^2 CFU/mL	[35]
Antibody-G-CR/FET	30 min	*E. coli*	10 CFU/mL	[19]
Antibody-Au-Al_2O_3-rGO FET	50 s	*E. coli*	10^3 CFU/mL	[18]
Phage-rGO-CR	30 min	*E. coli*	45 CFU/mL	This work

the resistance after the addition and 30 min of incubation of *E. coli* bacteria) was measured after the incubation with 20 μL of *E. coli* bacteria aliquots for 30 min followed by washing with PB (Fig. 5). As shown in the figure, a linear decrease in the device resistance was observed with the increase of *E. coli* concentration. This can be explained by the electrostatic gating effect induced by negatively charged *E. coli* (Fig. 6). When M13 phage captured the negatively charged *E. coli*, the density of negative surface changes was increased, which leads to an increase in the amount of hole carriers in the p-type rGO sheets. As shown in Fig. 5, the biosensor response exhibited an excellent linear correlation to Log_{10}(CFU/mL) over the complete tested concentration range ($R^2 = 0.9869$). The limit of detection (LOD), defined as LOD = 3*Sd/S, where Sd is the standard deviation of the mean of blank measurements, and S is the slope of the calibration curve, was estimated as 45 CFU/mL, which is competitive to other reports detecting bacteria by various detection methods (Table 1). Thakur et al.'s work on detection of *E. coli*, using antibody-Au-Al_2O_3-rGO, had a single cell detection in 1 μL, which is equivalent to 10^3 CFU/mL [18], which is slightly higher than the LOD of this sensor platform (45 CFU/mL). In addition, the introduced sensor implements M13 phage as a bioreceptor, which has a higher stability than the antibody-based biosensors. These results prove the M13 phage rGO-CR biosensor to be a strong candidate system for the detection of coliforms in water.

3.4. SEM imaging of E. coli cells captured by the biosensor

To verify that the increased response of the sensor system was derived from the phage-*E. coli* binding, two different concentrations of *E. coli* (10^3 and 10^6 CFU/mL) were incubated with two sensor chips for 30 min, washed with PB, and then imaged with SEM. The bacteria were captured by M13 phage on the electrodes which were totally covered by a thin film of rGO. The images in Fig. 7 show a clear difference in the number of bacteria between the two concentrations on the two chips. This confirms that the increase in sensor's resistance is attributed to the increase in number of captured bacterial cells.

3.5. Selectivity and control experiments

To test the selectivity of the proposed sensor, control experiments were designed (Fig. 8). Firstly, *P. Chlororaphis* was tested as non-host cells with M13-rGO sensor, and there was no noticeable response. Moreover, as a control experiment, the sensor without M13 phage was tested against *E. coli XL1-blue*. There was also no noticeable response detected. Thus, this sensor system is selective to F-pili of *E. coli* strains such as *XL1-blue*.

4. Conclusion

In this study, we reported the rGO-FET M13 phage-based biosensor system for early detection of *E. coli*. The interdigitated gold electrodes were modified with a thin film of rGO as a semiconductor sensing material. For the biorecognition element, M13 phage, a non-lytic and highly stable bacteriophage, was introduced for the selective recognition of F-pili containing *E. coli* strains. The developed sensor showed good sensitivity to detect *E. coli* strain with a LOD of 45 CFU/mL. This value is comparable with other methods which have been previously reported for detecting *E. coli*. Furthermore, this sensor was specific towards target bacteria and not affected by interference with other bacteria. From these observations, we concluded that the introduced sensor has a high sensitivity, and it showed selectivity to *E. coli*. This sensing system could be a promising platform for economic and accurate on-site detection of fecal coliforms with simple operations.

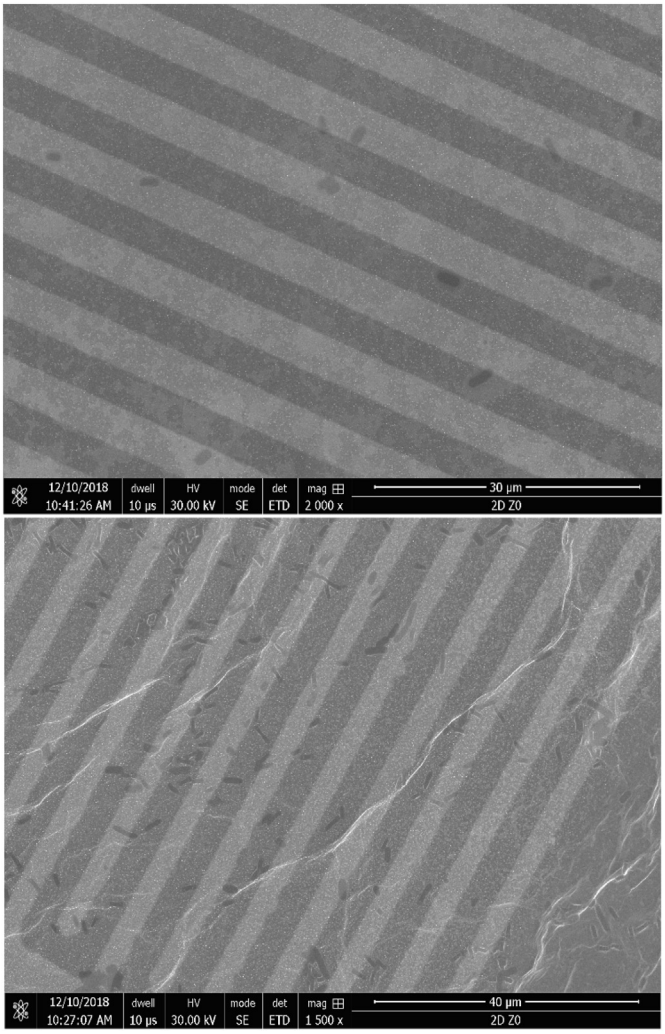

Fig. 7. SEM micrographs of the fabricated sensor chip incubated with *E. coli* bacteria at 10^3 CFU/mL (top) and 10^6 CFU/mL (bottom).

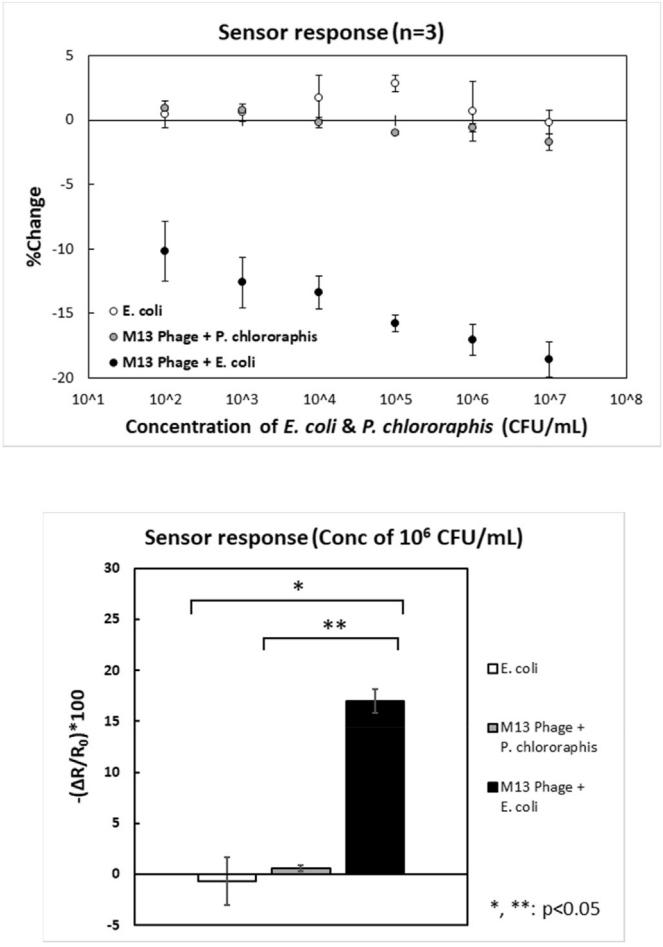

Fig. 8. Control experiments. (a) Calibration curves plotting % resistance change against the concentration of *P. chlororaphis*, as non-host bacteria to M13 phage (gray) compared to *E. coli* (black), as host bacteria. The white column shows the response of the sensor incubated with *E. coli* in the absence of M13 phage. (b) Responses at the bacteria concentration of 10^6 CFU/mL show no detectable response of the system with *P. chlororaphis* (in presence of M13 phage), with *E. coli* in presence and absence of M13 phage. The P value was <0.05. Each data point is an average of responses from 3 different M13-modified sensors and error bars represent ±1 standard deviation.

CRediT authorship contribution statement

Kenta Nakama: Conceptualization, Methodology, Formal analysis, Investigation, Writing - original draft, Writing - review & editing, Visualization. **Mohammed Sedki:** Conceptualization, Methodology, Formal analysis, Investigation, Writing - original draft, Writing - review & editing, Visualization. **Ashok Mulchandani:** Conceptualization, Methodology, Resources, Writing - review & editing, Supervision, Project administration, Funding acquisition.

Declaration of competing interest

The authors declare that they have no known competing financial interests or personal relationships that could have appeared to influence the work reported in this paper.

Acknowledgements

We acknowledge the financial support from DST/Intel®/Indo-U.S. Science and Technology Forum, W. Ruel Johnson Chair and Japan Student Services Organization.

References

[1] C. Dye, After 2015: infectious diseases in a new era of health and development, Phil. Trans. R. Soc. B 369 (2014) 20130426.
[2] J.T. Keer, L. Birch, Molecular methods for the assessment of bacterial viability, J. Microbiol. Methods 53 (2003) 175–183.
[3] F.v. Wintzingerode, U.B. Göbel, E. Stackebrandt, Determination of microbial diversity in environmental samples: pitfalls of PCR-based rRNA analysis, FEMS Microbiol. Rev. 21 (1997) 213–229.
[4] B. Byrne, E. Stack, N. Gilmartin, R. O'Kennedy, Antibody-based sensors: principles, problems and potential for detection of pathogens and associated toxins, Sensors 9 (2009) 4407–4445.
[5] D. V Lim, J.M. Simpson, E.A. Kearns, M.F. Kramer, Current and developing technologies for monitoring agents of bioterrorism and biowarfare, Clin. Microbiol. Rev. 18 (2005) 583–607.
[6] R.Y.A. Hassan, U. Wollenberger, Mediated bioelectrochemical system for biosensing the cell viability of Staphylococcus aureus, Anal. Bioanal. Chem. 408 (2016) 579–587.
[7] J. Xu, Y. Chau, Y. Lee, Phage-based electrochemical sensors: a review,, Micromachines 10 (2019) 855.
[8] J. Paczesny, Ł. Richter, R. Hołyst, recent progress in the detection of bacteria using bacteriophages: a review,, Viruses 12 (2020) 845.
[9] J. Rakonjac, M. Russel, S. Khanum, S.J. Brooke, M. Rajič, Filamentous phage: structure and biology, in: Antibodies Infect. Dis Recomb, Springer, 2017, pp. 1–20.
[10] M. Sedki, X. Chen, C. Chen, X. Ge, A. Mulchandani, Non-lytic M13 phage-based highly sensitive impedimetric cytosensor for detection of coliforms, Biosens, Bioelectron 148 (2020) 111794.
[11] C. García-Aljaro, L.N. Cella, D.J. Shirale, M. Park, F.J. Muñoz, M.V. Yates, A. Mulchandani, Carbon nanotubes-based chemiresistive biosensors for detection of microorganisms, Biosens, Bioelectron 26 (2010) 1437–1441.
[12] B.K. Das, C. Tlili, S. Badhulika, L.N. Cella, W. Chen, A. Mulchandani, Single-walled carbon nanotubes chemiresistor aptasensors for small molecules: picomolar level detection of adenosine triphosphate, Chem. Commun. 47 (2011) 3793–3795.
[13] M. Park, L.N. Cella, W. Chen, N. V Myung, A. Mulchandani, Carbon nanotubes-based chemiresistive immunosensor for small molecules: detection of nitro-aromatic explosives, Biosens. Bioelectron. 26 (2010) 1297–1301.
[14] C. Tlili, N. V Myung, V. Shetty, A. Mulchandani, Label-free, chemiresistor immunosensor for stress biomarker cortisol in saliva, Biosens. Bioelectron. 26 (2011) 4382–4386.
[15] W. Zhao, Y. Xing, Y. Lin, Y. Gao, M. Wu, J. Xu, Monolayer graphene chemiresistive biosensor for rapid bacteria detection in a microchannel, Sensors and Actuators Reports 2 (2020) 100004.
[16] M. Hatada, T.-T. Tran, W. Tsugawa, K. Sode, A. Mulchandani, Affinity sensor for haemoglobin A1c based on single-walled carbon nanotube field-effect transistor and fructosyl amino acid binding protein, Biosens. Bioelectron. 129 (2019) 254–259.
[17] L.G. Guex, B. Sacchi, K.F. Peuvot, R.L. Andersson, A.M. Pourrahimi, V. Ström, S. Farris, R.T. Olsson, Experimental review: chemical reduction of graphene oxide (GO) to reduced graphene oxide (rGO) by aqueous chemistry, Nanoscale 9 (2017) 9562–9571.
[18] B. Thakur, G. Zhou, J. Chang, H. Pu, B. Jin, X. Sui, X. Yuan, C.-H. Yang, M. Magruder, J. Chen, Rapid detection of single E. coli bacteria using a graphene-based field-effect transistor device, Biosens. Bioelectron. 110 (2018) 16–22.
[19] Y. Huang, X. Dong, Y. Liu, L.-J. Li, P. Chen, Graphene-based biosensors for detection of bacteria and their metabolic activities, J. Mater. Chem. 21 (2011) 12358–12362.
[20] M. Sedki, R.Y.A. Hassan, A. Hefnawy, I.M. El-Sherbiny, Sensing of bacterial cell viability using nanostructured bioelectrochemical system: rGO-hyperbranched chitosan nanocomposite as a novel microbial sensor platform, Sensors Actuators, Biol. Chem. 252 (2017), https://doi.org/10.1016/j.snb.2017.05.163.
[21] J. Ou, J. Wang, S. Liu, B. Mu, J. Ren, H. Wang, S. Yang, Tribology study of reduced graphene oxide sheets on silicon substrate synthesized via covalent assembly, Langmuir 26 (2010) 15830–15836.
[22] M. Sedki, M.B. Mohamed, M. Fawzy, D.A. Abdelrehim, M.M.S.A. Abdel-Mottaleb, Photosynthesis of silver-reduced graphene oxide (Ag-RGO) nanocomposite with an enhanced antibacterial effect using Potamogeton pectinatus extract, RSC Adv. 5 (2015) 17358–17365, https://doi.org/10.1039/c4ra13117g.
[23] M. Ciszewski, A. Mianowski, P. Szatkowski, G. Nawrat, J. Adamek, Reduced graphene oxide–bismuth oxide composite as electrode material for supercapacitors, Ionics 21 (2015) 557–563.
[24] D. Krishnan, F. Kim, J. Luo, R. Cruz-Silva, L.J. Cote, H.D. Jang, J. Huang, Energetic graphene oxide: challenges and opportunities, Nano Today 7 (2012) 137–152.
[25] S. Tian, J. Sun, S. Yang, P. He, S. Ding, G. Ding, X. Xie, Facile thermal annealing of graphite oxide in air for graphene with a higher C/O ratio, RSC Adv. 5 (2015) 69854–69860.
[26] D. Chen, L. Li, L. Guo, An environment-friendly preparation of reduced graphene oxide nanosheets via amino acid, Nanotechnology 22 (2011) 325601.
[27] D. Li, M.B. Müller, S. Gilje, R.B. Kaner, G.G. Wallace, Processable aqueous dispersions of graphene nanosheets, Nat. Nanotechnol. 3 (2008) 101.

[28] S. Yang, W. Yue, D. Huang, C. Chen, H. Lin, X. Yang, A facile green strategy for rapid reduction of graphene oxide by metallic zinc,, RSC Adv. 2 (2012) 8827–8832.
[29] J.I. Paredes, S. Villar-Rodil, P. Solís-Fernández, A. Martínez-Alonso, J.M.D. Tascon, Atomic force and scanning tunneling microscopy imaging of graphene nanosheets derived from graphite oxide, Langmuir 25 (2009) 5957–5968.
[30] P. Huang, C. Xu, J. Lin, C. Wang, X. Wang, C. Zhang, X. Zhou, S. Guo, D. Cui, Folic acid-conjugated graphene oxide loaded with photosensitizers for targeting photodynamic therapy, Theranostics 1 (2011) 240.
[31] H. Mohr, B. Lambrecht, A. Bayer, H. Spengler, S. Nicol, T. Montag, T.H. Müller, Basics of flow cytometry–based sterility testing of platelet concentrates, Transfusion 46 (2006) 41–49.
[32] M. Schmidt, Comparison of different methods of bacterial detection in blood components, ISBT Sci. Ser. 4 (2009) 80–86.
[33] P. Qi, D. Zhang, Y. Sun, Y. Wan, A selective near-infrared fluorescent probe for hydrogen sulfide and its application in sulfate-reducing bacteria detection, Anal, Methods 8 (2016) 3339–3344.
[34] J. Chang, S. Mao, Y. Zhang, S. Cui, G. Zhou, X. Wu, C.-H. Yang, J. Chen, Ultrasonic-assisted self-assembly of monolayer graphene oxide for rapid detection of Escherichia coli bacteria, Nanoscale 5 (2013) 3620–3626.
[35] G. Wu, Z. Dai, X. Tang, Z. Lin, P.K. Lo, M. Meyyappan, K.W.C. Lai, Graphene field-effect transistors for the sensitive and selective detection of Escherichia coli using pyrene-tagged DNA aptamer, Adv. Healthc. Mater 6 (2017) 1700736.